J. Fluid Mech. (1991), *vol.* 232, *pp.* 21–45
Printed in Great Britain

Flow past a constriction in a channel: a modal description

By G. G. TOMASSON AND W. K. MELVILLE
R. M. Parsons Laboratory, Massachusetts Institute of Technology, Cambridge, MA 02139, USA

(Received 14 August 1990 and in revised form 12 April 1991)

We consider the waves generated by transcritical flow past a constriction in a channel, or by ships or surface pressure distributions travelling at transcritical speeds. The two-dimensionality of the upstream advancing nonlinear waves, which has been observed both experimentally and numerically by several authors, is described by a modal decomposition of the flow response. We show that the lowest transverse mode may evolve nonlinearly, leading to a two-dimensional response upstream, with the higher transverse modes swept downstream. This description is supported by comparing the initial evolution of the solutions to the corresponding linear and nonlinear problems. Averaging across the channel demonstrates that the three-dimensional problem may be related to the corresponding two-dimensional problem with an additional effective forcing coming from the nonlinear coupling of the higher modes to the lowest two-dimensional mode. This coupling leads to a dependence of the upstream solutions on the channel width as well as the Froude number. Solutions are also obtained for two-layer fluids in which cubic nonlinearity is also important. The inclusion of cubic nonlinearity permits the generation of two-dimensional fronts upstream, and demonstrates that the transition from three- to two-dimensional solutions upstream is not specific to Boussinesq solitary waves.

1. Introduction

The generation of long nonlinear waves in a channel by flow over and past topography, and by travelling disturbances such as ships or surface pressure perturbations, has aroused considerable interest in recent years. Of particular interest has been the wave field generated when a characteristic Froude number is near unity. Linear theory predicts unbounded growth of the disturbance when the Froude number is exactly unity. The introduction of the effects of nonlinearity and dispersion restores the boundedness of the disturbance and may lead to the generation of nonlinear waves upstream. Experimental results by Huang *et al.* (1982) and Ertekin, Webster & Wehausen (1984) were among the first to show trains of solitary waves propagating upstream of ships moving at transcritical speeds in a channel. Ertekin (1984) also reports on waves upstream for subcritical Froude numbers. However, as described below, the generation mechanism for this case is different from that for the transcritical Froude numbers, which is the main focus of this paper.

A number of authors, among them Wu & Wu (1982), Akylas (1984) and Mei (1986), have solved the two-dimensional problem numerically. Their results are consistent with the experimental findings, showing solitons being radiated upstream of the forcing. The generation of the upstream nonlinear waves in the transcritical range can be understood in the following way. When the speed of the forcing is close to

critical (i.e. close to the phase speed of the linear waves), the fluid is being forced near resonance and energy is continuously transferred from the moving disturbance to the fluid. In addition, owing to the weak dispersive effects, the group velocity of the linear waves is also close to the velocity of the forcing, thus energy cannot radiate away, resulting in a growth of the leading disturbance in the linear problem. However, as the amplitude becomes finite, nonlinear effects become important and nonlinear waves are generated. Grimshaw & Smyth (1986) and later Smyth (1987), considering a forced Korteweg–de Vries (KdV) equation, were able to predict analytically the main characteristics of the upstream solution based on the size of the topographic forcing and the Froude number. Their predictions of the amplitude and period of generation of the upstream advancing solitons, together with the Froude-number range in which these resonance effects occur, compared well with numerical solutions.

In an experimental and numerical study, Melville & Helfrich (1987) considered the two-dimensional problem of a transcritical flow over bottom topography in a two-layer fluid. They too observed upstream advancing solitons for cases where the KdV equation applies; their results agreeing moderately well with the analytical predictions of Grimshaw & Smyth (1986) and Smyth (1987). However, in a certain parametric range of the two-layer problem, cubic nonlinearity is comparable to quadratic nonlinearity and cannot be neglected. The appropriate evolution equation is then the extended KdV (EKdV) equation. Melville & Helfrich (1987) found that this changes the character of the upstream disturbance, giving an upstream advancing non-dissipative bore, rather than a train of Boussinesq solitary waves.

A striking feature of many of the experimental results is the two-dimensionality of the upstream waves, which are straight crested and uniform across the channel, even though the forcing is three-dimensional. Several authors have considered the three-dimensional problem, both analytically and numerically. Mei (1986) showed that for channel widths W, satisfying $kW = O(\beta^{-\frac{1}{4}})$, where k^{-1} is the lengthscale in the longitudinal direction, $\beta = (kh)^2 \ll 1$ is the dispersion parameter, and h is the water depth, the problem can be treated as essentially two-dimensional. The truly three-dimensional problem (i.e. $kW = O(\beta^{-\frac{1}{2}})$) has been considered by several authors, including Ertekin, Webster & Wehausen (1986) and Katsis & Akylas (1987). Their numerical solutions show two-dimensional solitons being radiated upstream of the three-dimensional forcing for transcritical Froude numbers. Katsis & Akylas related the two-dimensionality of the upstream waves to the stability of the two-dimensional solitary wave solution. Most recently, Pedersen (1988) has solved the three-dimensional problem using Boussinesq-type equations forced by either a travelling pressure distribution or a time-dependent bottom topography. His numerical results show relatively good agreement with the experimental results of Ertekin *et al.* (1984), with the amplitude of the upstream advancing solitons determined by the blockage coefficient, which measures the strength of the forcing (see also Macomb 1986) and the Froude number. However, in contrast to the experimental results and the analytical predictions of Grimshaw & Smyth (1986), Smyth (1987) and Wu (1987) for the two-dimensional case, he concludes that neither the period of soliton generation nor the Froude-number range in which upstream influence occurs, is 'particularly related' to the blockage coefficient. Instead he postulates that a Mach-reflection mechanism at the sidewall of the channel is responsible for the generation of the two-dimensional upstream solitons from the three-dimensional disturbance, with the characteristics of the Mach reflection determining the maximum Froude number at which upstream influence is possible.

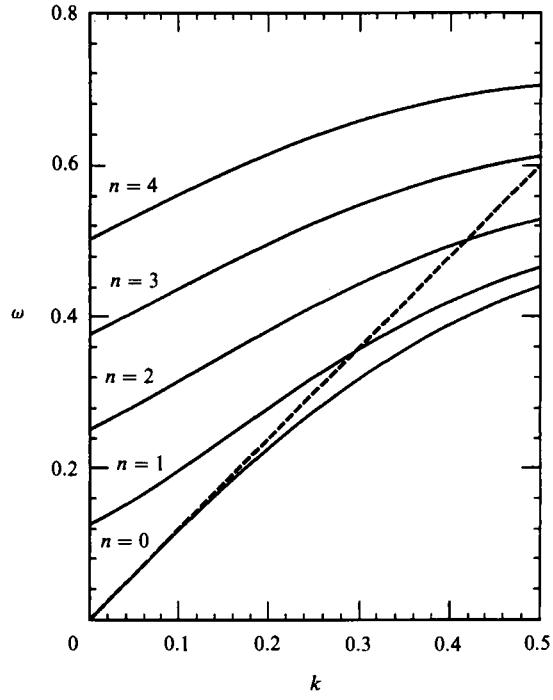

FIGURE 1. The dispersion relationship of ——, the linear modes and – – –, the forcing travelling at the critical speed, $F = 1$. Here ω is scaled by c_0/h, k is scaled by h.

In the present work we describe the two-dimensionality of the upstream disturbances using the dynamics of the transverse modes of the channel, rather than the properties of nonlinear reflection. In figure 1 we show the dispersion relationship of the linear transverse modes of the channel (defined in §2), together with the locus of a disturbance travelling at a transcritical speed. Here we have chosen $kW = O(\beta^{-\frac{1}{2}})$, so that transverse effects are important, which is manifested by the fact that the forcing curve lies close to and even intersects the curves of the higher transverse modes ($n = 1, 2, \ldots$), within the wavenumber range of interest.

We immediately see that for the lowest transverse mode ($n = 0$) at small wavenumbers, both the phase and group velocities of the waves are close to the velocity of the forcing, resulting in the energy accumulating and nonlinear effects becoming important, as described above for the two-dimensional case. However, this does not apply to the higher transverse modes ($n = 1, 2, \ldots$). At small wavenumbers their group velocity is considerably less than that of the lowest mode and less than the speed of the forcing. At those wavenumbers where their phase velocity matches the velocity of the forcing (resulting in a resonance), their group velocity is again considerably less than the velocity of the forcing. Thus their energy is swept downstream with the flow, rather than accumulating as is the case for the lowest mode. This essentially explains the two-dimensionality of the leading disturbance: the lowest transverse mode is the only one that independently evolves nonlinearly and generates upstream propagating waves. In §4 we support this argument by comparing linear solutions of the problem to corresponding nonlinear ones, for both subcritical and transcritical Froude numbers. In the subcritical case, linear transients propagate upstream of the forcing region and then evolve nonlinearly; in contrast, the upstream influence in the transcritical case is due to nonlinear and resonant

effects, as described above. In §5 we give numerical results for the three-dimensional nonlinear problem at larger times and explain why the properties of the upstream waves are slightly different from those of the corresponding two-dimensional case (see Appendix B for a definition of the corresponding two-dimensional problem); showing that the properties of the upstream waves depend both on the blockage coefficient and the width of the three-dimensional channel, as well as the Froude number.

We also extend the work of Melville & Helfrich (1987) for the two-layer internal wave problem to a three-dimensional channel. In certain parametric regions, where cubic nonlinearity cannot be neglected, the upstream disturbance is a monotonic bore, rather than a train of Boussinesq solitary waves. In §6 we show that the solutions for the two-layer case including the cubic nonlinearity differ little from those given in §4 for the linear problem and those given in §5 for the quadratic nonlinear problem up to times at which the leading disturbance has reflected from the far wall and nonlinear effects become important; again confirming the usefulness of the modal description of the problem. Numerical solutions for larger times are given and compared to results of the corresponding two-dimensional problem.

2. Evolution equations

The evolution equations for long, weakly nonlinear three-dimensional waves in a channel are derived following the procedure outlined by Melville & Helfrich (1987) and Helfrich & Melville (1990) (see also Grimshaw & Melville 1989). We consider a sidewall perturbation moving with a constant speed through a two-layer, inviscid and incompressible stationary fluid bounded by a rigid lid above. This is equivalent to the problem of a steady uniform flow past a fixed constriction. The coupled evolution equations for waves moving to the right are

$$\eta_t+\eta_x+\tfrac{3}{2}\alpha[d_{-2}\,\eta-2\alpha d_{-3}\,\eta^2]\,\eta_x-\tfrac{1}{6}\beta d_1\,\eta_{xxt}+\tfrac{1}{2}\Gamma V_y=0, \tag{2.1a}$$

$$V_t+\eta_y=0. \tag{2.1b}$$

Here η is the displacement of the interface from its equilibrium position and V is the transverse flux in the upper layer. The three small parameters are

$$\alpha=\frac{a}{h_0},\quad \beta=(kh_0)^2,\quad \Gamma=\left(\frac{l}{k}\right)^2, \tag{2.2}$$

representing weak nonlinearity, weak dispersion and weak transverse effects, respectively. All variables have been made dimensionless through the transformation

$$\left.\begin{aligned} x^*=k^{-1}x,\quad y^*=l^{-1}y,\quad t^*=(kc_0)^{-1}t,\\ \eta^*=a\eta,\quad V^*=ac_0\frac{l}{k}V,\quad d_\pm^*=h_0 d_\pm, \end{aligned}\right\} \tag{2.3}$$

where * refers to the dimensional variables. Here a is a typical amplitude of the interface disturbance, k^{-1} and l^{-1} are typical lengthscales in the along-channel and across-channel directions, $d_\pm$ are the upper- and lower-layer depths, $h_0=d_+^*d_-^*/(d_+^*+d_-^*)$ is an equivalent single-layer depth, $d_n=\{d_-^n+(-1)^{n-1}d_+^n\}$ and $c_0^2=(\Delta\rho/\rho)gh_0$.

The sidewall boundary condition is

$$V = -\frac{F}{\alpha\Gamma}\frac{\mathrm{d}}{\mathrm{d}\xi}(Y_- - Y_+) = -F\frac{B}{\alpha\Gamma}\frac{\mathrm{d}Y}{\mathrm{d}\xi} \quad \text{at } y = 0, \tag{2.4a}$$

$$V = 0 \quad \text{at } y = W, \tag{2.4b}$$

where F is the Froude number, $F = U/c_0$, U is the speed of the constriction, $BY = Y_- - Y_+$, where B is the dimensionless maximum amplitude of $Y_- - Y_+$, with $B = O(\alpha\beta)$ and $Y = O(1)$, $y = Y_\pm(\xi)$ defines the sidewall boundary in the upper and lower layers, $\xi = x - Ft$ and W is the width of the channel. For simplicity we assume the constriction to have piecewise vertical walls in the two layers. With this assumption the internal mode considered here is excited by the difference between the width of the constriction in each layer, the depth-averaged width excites the surface mode, which is neglected here by the assumption of a rigid lid (Melville & Macomb 1987). In all the solutions presented here we used

$$Y = \operatorname{sech}^2\left[\frac{\xi}{L}\right]. \tag{2.5}$$

The linearized version of (2.1*a*, *b*), transformed into a problem with homogeneous boundary conditions, can be decomposed into a set of transverse modes defined by

$$\left.\begin{aligned} V_n(x,y,t) &= \hat{V}_n(x,t)\sin\left[\frac{n\pi y}{W}\right] && (2.6a)\\ \eta_n(x,y,t) &= \hat{\eta}_n(x,t)\cos\left[\frac{n\pi y}{W}\right] && (2.6b) \end{aligned}\right\} \quad (n = 0, 1, 2, \ldots),$$

with the linear dispersion relationship given by

$$\omega^2(1 + \tfrac{1}{6}\beta d_1 k^2) - \omega k - \tfrac{1}{2}\Gamma\left(\frac{n\pi}{W}\right)^2 = 0, \tag{2.7}$$

where we have taken $\hat{\eta}_n, \hat{V}_n \sim \mathrm{e}^{\mathrm{i}(kx-\omega t)}$. The transverse modal functions form a complete and orthogonal set and will be used to describe both linear and nonlinear solutions of the problem.

If $d_{-2} = O(1)$, the cubic nonlinear term can be neglected compared to the quadratic one, with the balance in the equations given by $\beta = O(\Gamma) = O(\alpha)$. This is equivalent to the single-layer case provided that the blockage coefficient for the two-layer case is defined to be

$$S = \frac{B}{W}d_{-2}, \tag{2.8}$$

as is shown in Appendix A. These equations are a two-dimensional extension of the KdV equation and admit the well-known solitary wave solutions (independent of y)

$$\eta = A\operatorname{sech}^2[\lambda^{-1}(x - ct)], \tag{2.9a}$$

where A is an arbitrary amplitude, the lengthscale and speed are

$$\lambda = \left[\frac{4}{3}\frac{\beta d_1}{\alpha d_{-2} A}\right]^{\frac{1}{2}}, \tag{2.9b}$$

and

$$c = 1 + \tfrac{1}{2}\alpha d_{-2} A. \tag{2.9c}$$

If on the other hand we have $d_{-2} = O(\alpha) \ll 1$, the cubic nonlinear term cannot be neglected and the balance in the equations is $\beta = O(\Gamma) = O(\alpha^2)$. The equations are then a two-dimensional extension of the EKdV. These equations admit a family of solitary wave solutions similar to the ones given above. However, of more interest here is another solution found by Kakutani & Yamasaki (1978) and Miles (1979)

$$\eta = A\tfrac{1}{2}\{1+\tanh[\lambda^{-1}(x-ct)]\}, \tag{2.10a}$$

where A is now a predetermined amplitude

$$A = \frac{d_{-2}}{2\alpha d_{-3}} = O(1), \tag{2.10b}$$

with the lengthscale and speed given by

$$\lambda = \left[\frac{16}{3}\frac{\beta d_1 d_{-3}}{d_{-2}^2}\right]^{\frac{1}{2}} = O(1), \tag{2.10c}$$

and

$$c = 1+\frac{1}{8}\frac{d_{-2}^2}{d_{-3}} = 1+O(\alpha^2), \tag{2.10d}$$

respectively.

The coupled evolution equations (2.1a, b) may be reduced to a single equation by assuming that

$$V_t = -V_x+O(\beta) \tag{2.11}$$

in (2.1b) to give

$$-V_x+\eta_y = 0. \tag{2.12}$$

Cross differentiating (2.1a) and (2.12) and adding gives

$$[\eta_t+\eta_x+\tfrac{3}{2}\alpha[d_{-2}\eta-2\alpha d_{-3}\eta^2]\eta_x-\tfrac{1}{6}\beta d_1\eta_{xxt}]_x+\tfrac{1}{2}\Gamma\eta_{yy} = 0, \tag{2.13}$$

which is the extended KP equation and reduces to the KP equation used by Katsis & Akylas (1987) by neglecting the cubic nonlinear term (Grimshaw & Melville 1989).

3. Numerical scheme

For convenience in presenting the numerical scheme and the numerical solutions, we renormalize the equations so that all coefficients except that in the cubic nonlinear term become unity. The required scaling is

$$\left.\begin{gathered} x = (\tfrac{1}{6}\beta d_1)^{\frac{1}{2}}x', \quad y = (\tfrac{1}{12}\beta\Gamma d_1)^{\frac{1}{2}}y', \quad t = (\tfrac{1}{6}\beta d_1)^{\frac{1}{2}}t', \\ \eta = \frac{2}{3\alpha d_{-2}}t', \quad V = \left(\frac{2}{\Gamma}\right)^{\frac{1}{2}}\frac{2}{3\alpha d_{-2}}V', \end{gathered}\right\} \tag{3.1}$$

where the primed variables denote our new non-dimensional variables. Then the initial boundary-value problem becomes

$$\eta_t+\eta_x+(\eta-\gamma\eta^2)\eta_x-\eta_{xxt}+V_y = 0, \tag{3.2a}$$

$$V_t+\eta_y = 0, \tag{3.2b}$$

$$V(x,0,t) = -\tfrac{3}{4}FBd_{-2}Y_\xi, \quad V(x,W,t) = 0 \quad (t>0), \tag{3.2c}$$

$$\eta(x,y,0) = V(x,y,0) = 0, \tag{3.2d}$$

where $\gamma = \frac{4}{3}(d_{-3}/d_{-2}^2)$, and we have dropped the primes for convenience.

Winther (1983) developed a numerical scheme for these equations without the cubic nonlinear term (i.e. with $\gamma = 0$). The scheme is locally second-order accurate in both space and time, giving the difference equations

$$\frac{1}{\Delta t}(\eta_{i,j}^{n+1}-\eta_{i,j}^{n})+\frac{1}{4\Delta x}[(\eta_{i+1,j}^{n+1}+\eta_{i+1,j}^{n})-(\eta_{i-1,j}^{n+1}+\eta_{i-1,j}^{n})]$$

$$+\frac{1}{4\Delta x}[\eta_{i,j}^{n}(\eta_{i+1,j}^{n+1}+\eta_{i-1,j}^{n+1})+\eta_{i,j}^{n+1}(\eta_{i+1,j}^{n}+\eta_{i-1,j}^{n})]$$

$$-\frac{1}{\Delta t(\Delta x)^2}[(\eta_{i+1,j}^{n+1}-2\eta_{i,j}^{n+1}+\eta_{i-1,j}^{n+1})-(\eta_{i+1,j}^{n}-2\eta_{i,j}^{n}+\eta_{i-1,j}^{n})]$$

$$+\frac{1}{\Delta y}[V_{i,j+1}^{n}-V_{i,j}^{n}]=0, \tag{3.3a}$$

and

$$\frac{1}{\Delta t}[V_{i,j}^{n+1}-V_{i,j}^{n}]+\frac{1}{\Delta y}[\eta_{i,j}^{n+1}-\eta_{i,j-1}^{n+1}]=0, \tag{3.3b}$$

where

$$\eta_{i,j}^{n}=\eta[i\Delta x,(j+\tfrac{1}{2})\Delta y,n\Delta t], \tag{3.4a}$$

$$V_{i,j}^{n}=V[i\Delta x,j\Delta y,(n+\tfrac{1}{2})\Delta t]. \tag{3.4b}$$

The boundary and initial conditions are

$$\eta_{0,j}^{n+1}=\eta_{N_x,j}^{n+1}=0, \tag{3.5a}$$

$$V_{i,0}^{n+1}=\mathscr{V}_i^n, \tag{3.5b}$$

$$V_{i,N_y}^{n+1}=0, \tag{3.5c}$$

$$\eta_{i,j}^{0}=V_{i,j}^{0}=0. \tag{3.5d}$$

Winther (1983) showed that this scheme is stable if $\Delta t/\Delta y \leqslant 1$ and $(\Delta x)^4/\Delta y \downarrow 0$. Unless otherwise indicated, in all runs with $\gamma = 0$, we used a grid size $(\Delta x, \Delta y) = (0.25, 0.2)$ and $\Delta t = 0.2$.

The cubic nonlinear term is added to the scheme in the following way

$$\eta^2\eta_x=\frac{1}{6\Delta x}[2\eta_{i,j}^{n+1}\eta_{i,j}^{n}(\eta_{i+1,j}^{n}-\eta_{i-1,j}^{n})+(\eta_{i,j}^{n})^2(\eta_{i+1,j}^{n+1}-\eta_{i-1,j}^{n+1})], \tag{3.6}$$

which is only first-order accurate in space. Thus, to keep the second-order accuracy of the scheme, iterations are necessary. However, from numerical experimentation we found that by choosing $(\Delta x, \Delta y) = (0.25, 0.2)$ and $\Delta t = 0.125$, the scheme was sufficiently stable without iteration up to times well above those presented in §6. These values are used in all runs which included cubic nonlinearity. Tests on the propagation of the exact analytical solution given by (2.10), gave errors of less than 2% of the maximum amplitude after 15000 timesteps, which is comparable to the maximum number of timesteps used in the solutions presented in §6. Mass and energy were conserved to within 0.5% accuracy.

Truncation of the computational domain may require the specification of radiation conditions at the upstream and downstream boundaries. In this case the upstream solution is of primary interest and the computational domain was continuously

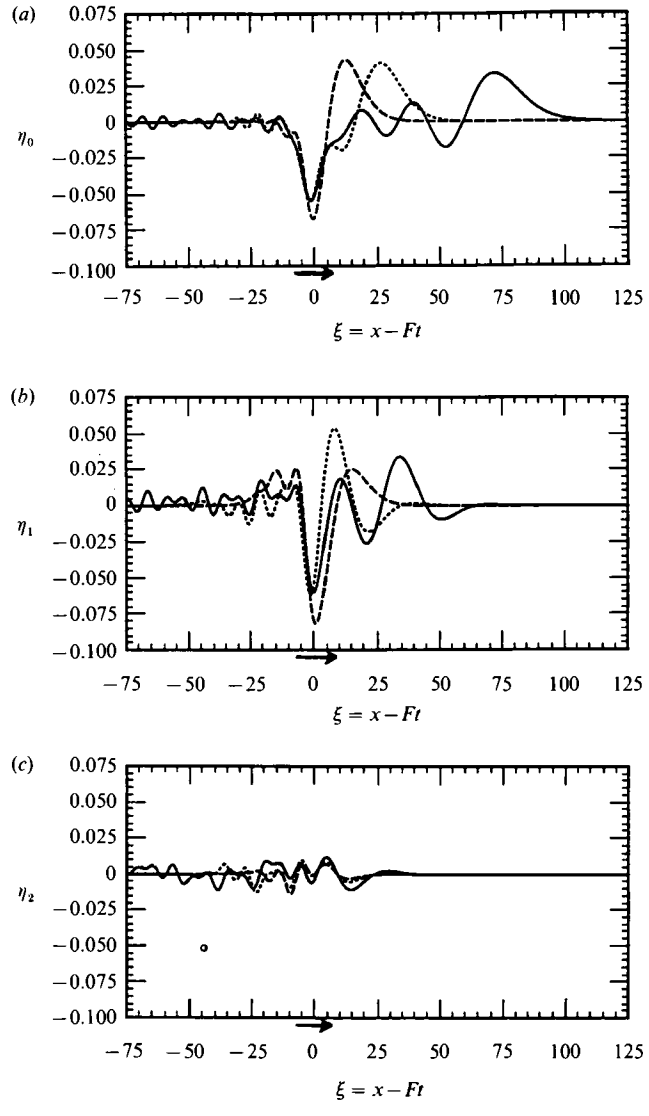

FIGURE 2. The linear solution for the subcritical case ($F = 0.6, S = 0.044, W = 40$), for the first three transverse modes of η at ——, $t = 40$; ---, $t = 80$ and ——, $t = 200$. (*a*) Zeroth mode, (*b*) 1st mode, (*c*) 2nd mode. The arrows indicate the location, size and direction of propagation of the sidewall constriction. In this and subsequent figures the scales are those defined by (3.1), unless otherwise stated.

extended to ensure that no disturbance reached this boundary. This procedure would be very time consuming in the case of the downstream boundary and instead the solution was weighted with a 'tanh' window so that the dependent variables and their derivatives approached zero sufficiently smoothly. This *ad hoc* procedure was tested and found only to give detectable differences (in contour plots of elevation) over a small fraction of the channel length closest to the downstream boundary.

4. Linear solutions

Before going on to describe numerical solutions to the full nonlinear problem, it is instructive to look at the corresponding linear problem in order to better understand the underlying physics. In fact, since the solution is started from a quiescent state, it remains essentially linear until it reaches a large enough amplitude for nonlinear effects to become important (see the discussion in §1).

To confirm this, we solve the linearized three-dimensional problem numerically and compare with the numerical solutions of the corresponding nonlinear problem (see §5). We will consider two cases, a subcritical case with $F = 0.6$ and a transcritical case with $F = 1.05$. In both cases we have taken the blockage coefficient to be $S = 0.044$ and the width of the channel to be $W = 40$. In figure 2 the linear solution for the lowest three transverse modes for the subcritical case is shown at three different times. We see a linear transient disturbance propagating upstream of the forcing with its leading part dominated by the lowest transverse mode, owing to its group velocity exceeding that of the higher modes, as discussed in §1. This can also be seen quite clearly in the contour plots of the full linear solution, shown in figure 3 along with its nonlinear counterparts, to be discussed in §5.

Figure 4 shows the solution for the lowest three transverse modes at three times for the transcritical case. We see that at the leading edge of the disturbance the lowest mode ($n = 0$) grows initially with time much like the solution to the corresponding two-dimensional problem, whereas the higher transverse modes are bounded in amplitude owing to their energy being swept downstream, as is apparent from the increasing length of the downstream tail. As the lowest mode grows with time, the leading edge of the disturbance becomes more uniform and straight crested across the channel. This can be seen in the contour plots of the full linear solution shown in figure 5 along with its nonlinear counterparts, to be discussed in §5.

The above arguments imply that in the transcritical range, only the lowest transverse mode, which corresponds to the only mode in the two-dimensional problem, will evolve nonlinearly upstream, with the nonlinear waves generated being essentially uniform and straight crested across the channel. The higher modes will not evolve nonlinearly upstream, owing to their energy being swept downstream. Thus, the prediction of the upstream disturbance generated by the three-dimensional transcritical flow past a constriction in a channel is reduced to solving the corresponding two-dimensional problem modified by nonlinear interactions of the lowest mode with the higher transverse modes, as will be shown in §5.

5. Results for quadratic nonlinearity

If $d_+ - d_- = O(d_+, d_-)$, the cubic nonlinear term can be neglected and the governing equations become (3.2) with $\gamma = 0$. These equations are solved numerically using the scheme described in §3.

In figure 3 we show contour plots of the nonlinear solutions of the subcritical case together with their linear counterparts. Qualitatively the two agree very well and quantitatively the agreement is good up to times at which the leading upstream disturbance starts to evolve nonlinearly. Note the excellent agreement between the two sets of solutions at those times at which the leading disturbance is reflecting from the far wall ($t \leqslant 80$).

In figure 5 we show contour plots of the nonlinear solutions to the transcritical case together with their linear counterparts. Again, the two agree quite well up to times

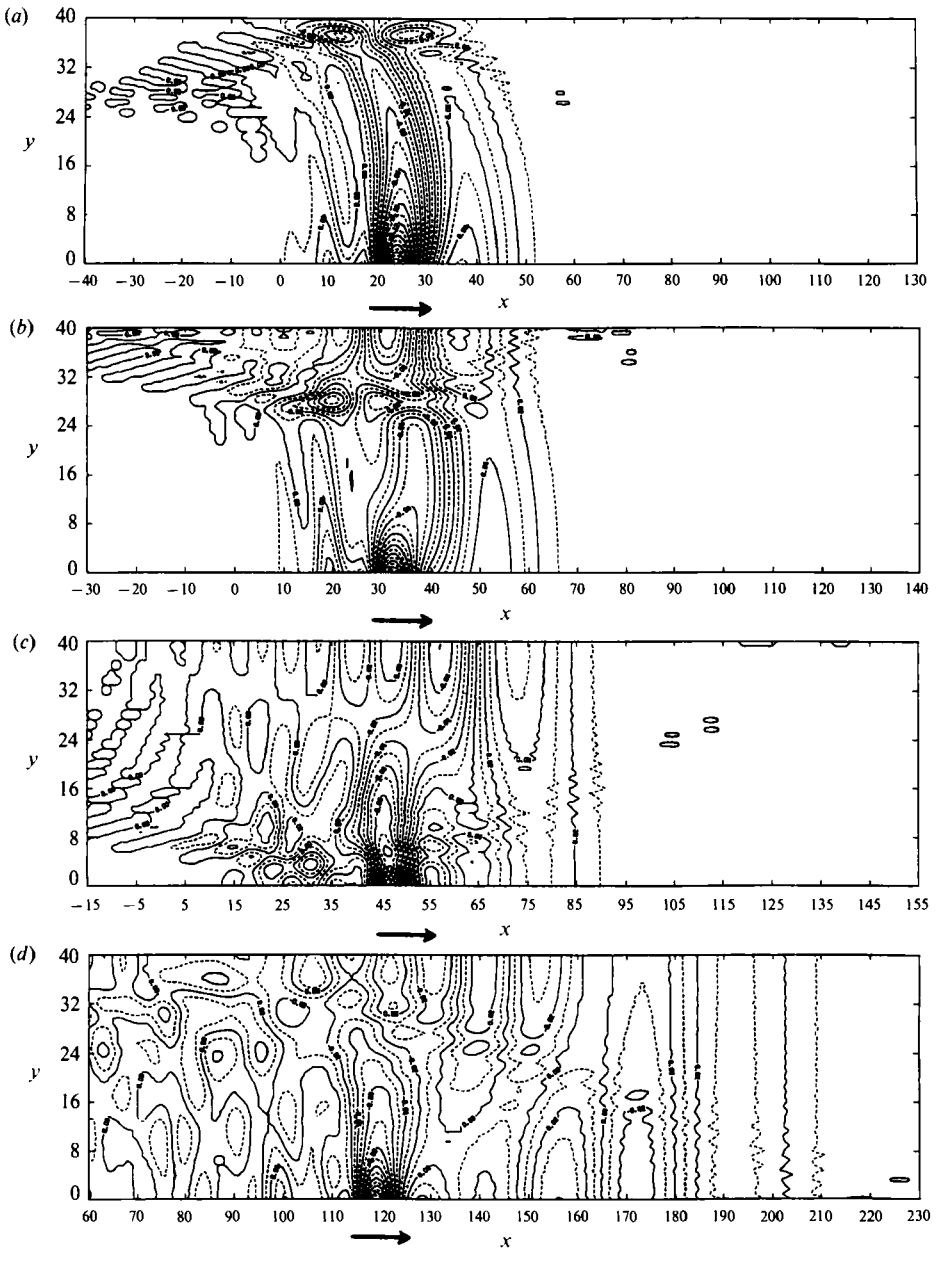

FIGURE 3(*a–d*). For caption see facing page.

at which nonlinear effects in the leading disturbance become apparent ($t > 80$). Note again the excellent agreement between the two at those times at which the leading disturbance is reflecting from the far wall. Also note the qualitative resemblance of this process to the Mach reflection, to which Pedersen (1988) attributed the generation of the upstream waves in the transcritical case. Here these qualitative effects appear in the linear solution and cannot be attributed to a nonlinear reflection process.

As a measure of the two-dimensionality of the leading disturbance, we have listed

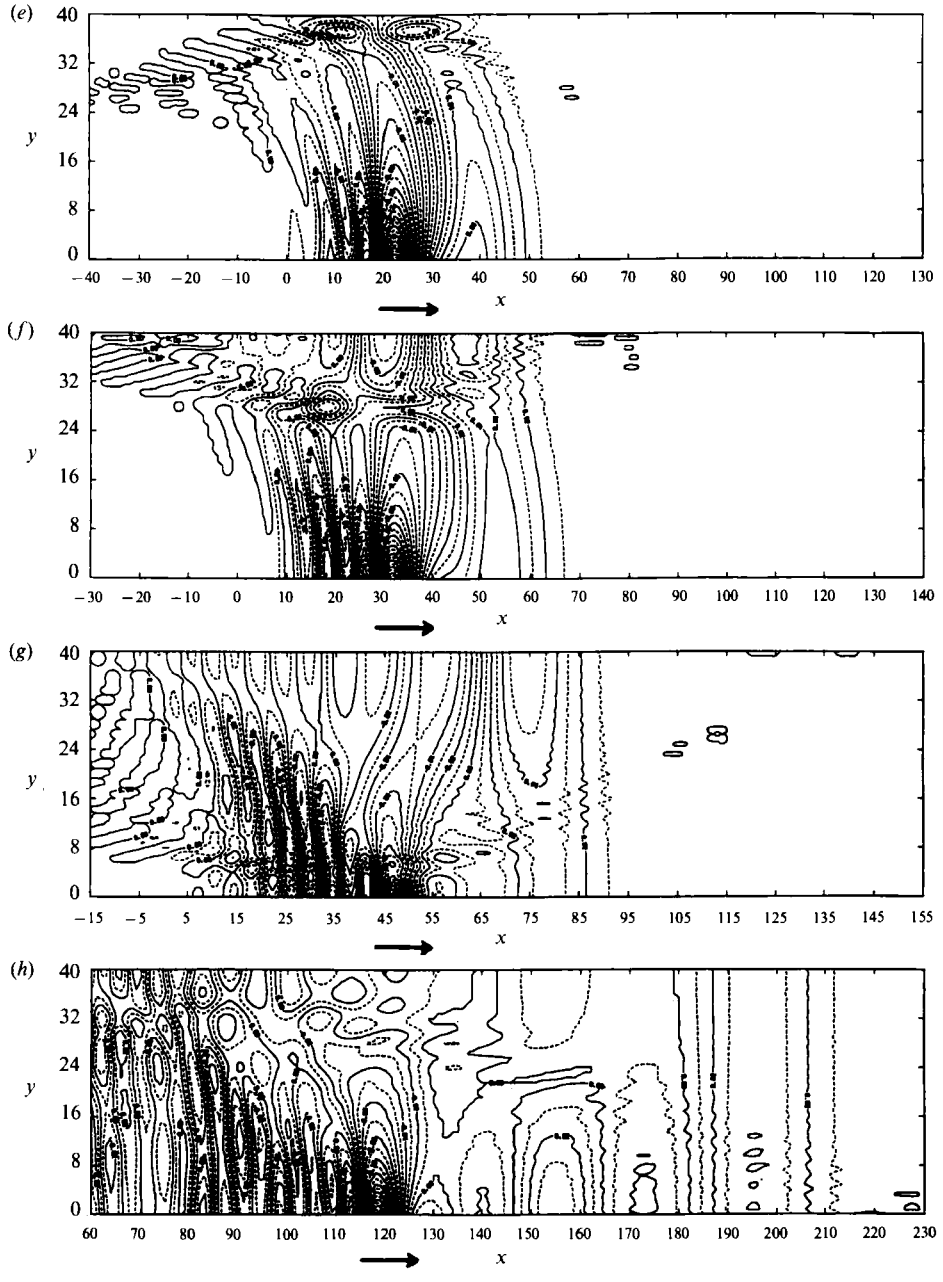

FIGURE 3. Contour plots of the linear and quadratic nonlinear solution for η for the subcritical case ($F = 0.6, S = 0.044, W = 40$). (*a*) Linear at $t = 40$; (*b*) linear at $t = 55$; (*c*) linear at $t = 80$; (*d*) linear at $t = 200$; (*e*) nonlinear at $t = 40$; (*f*) nonlinear at $t = 55$; (*g*) nonlinear at $t = 80$; (*h*) nonlinear at $t = 200$. The arrows indicate the location, size and direction of propagation of the sidewall constriction.

in table 1 the angle the leading crest makes at the centre of the channel with a line normal to the channel walls. As the nonlinear solution becomes exactly straight in the transcritical case at $t \approx 200$, the linear solution is still slightly curved. In this modal description, the transition to a nonlinear two-dimensional upstream

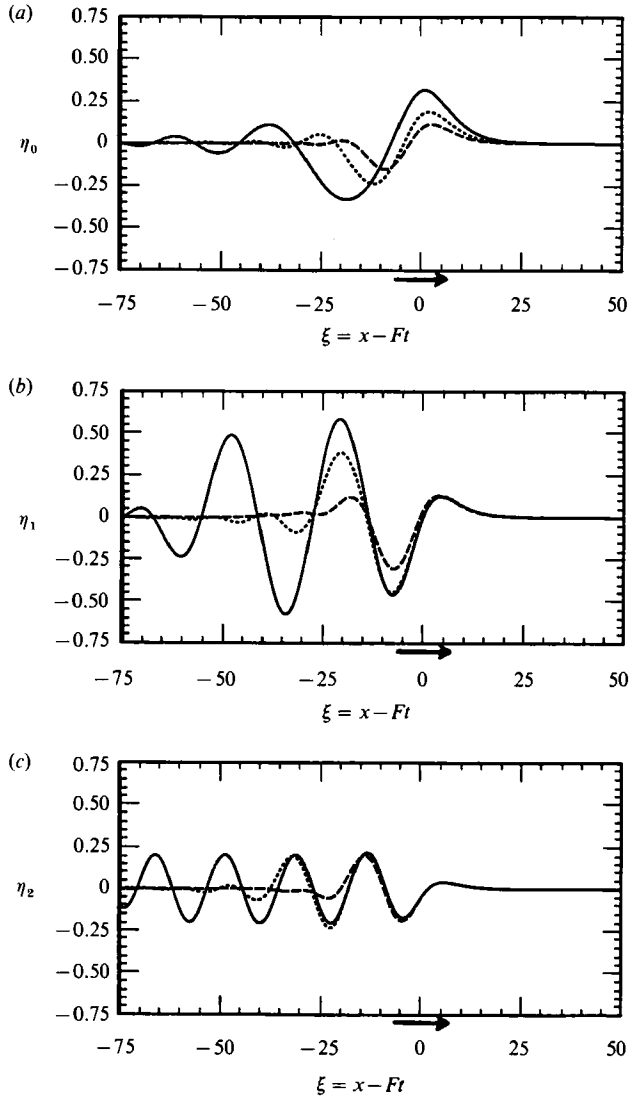

FIGURE 4. The linear solution for the transcritical case ($F = 1.05$, $S = 0.44$, $W = 40$) for the first three transverse modes of η at ———, $t = 40$; ---, $t = 80$ and ——, $t = 200$. (*a*) Zeroth mode, (*b*) 1st mode, (*c*) 2nd mode. The arrows indicate the location, size and direction of propagation of the sidewall constriction.

disturbance is due to the increase in speed of the nonlinear lowest mode, and its consequent propagation upstream of the forcing region, away from the higher transverse modes.

In the subcritical case the upstream influence was due to linear transients propagating upstream of the forcing owing to their group velocities exceeding the velocity of the forcing. However, in the transcritical range, the upstream propagating nonlinear waves are generated by the resonant forcing of the lowest transverse mode. Rather than growing to large amplitudes as in the corresponding linear problem, nonlinear effects become important and lead to a periodic generation of finite amplitude nonlinear waves, which propagate upstream of the forcing in certain

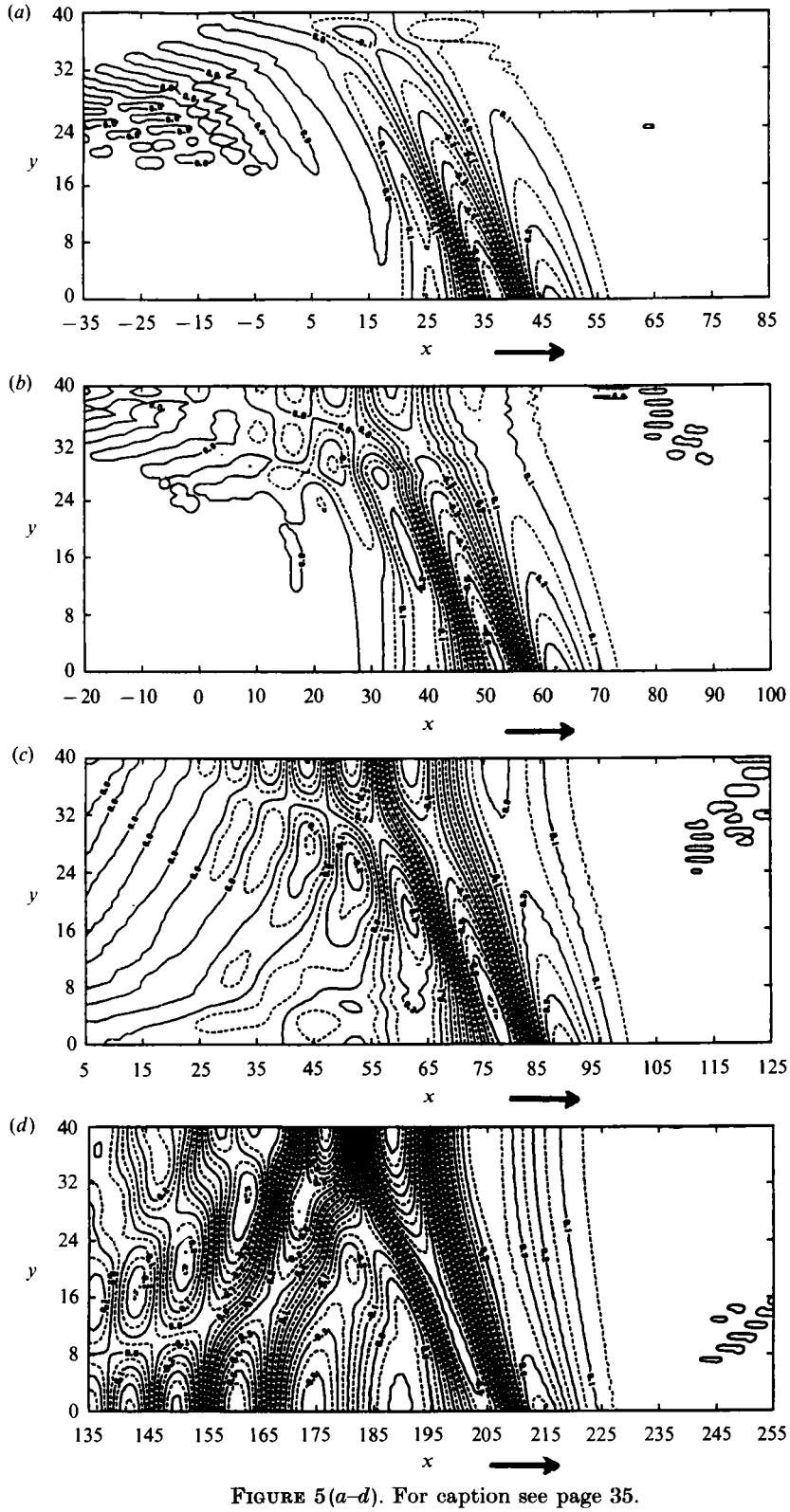

FIGURE 5(*a–d*). For caption see page 35.

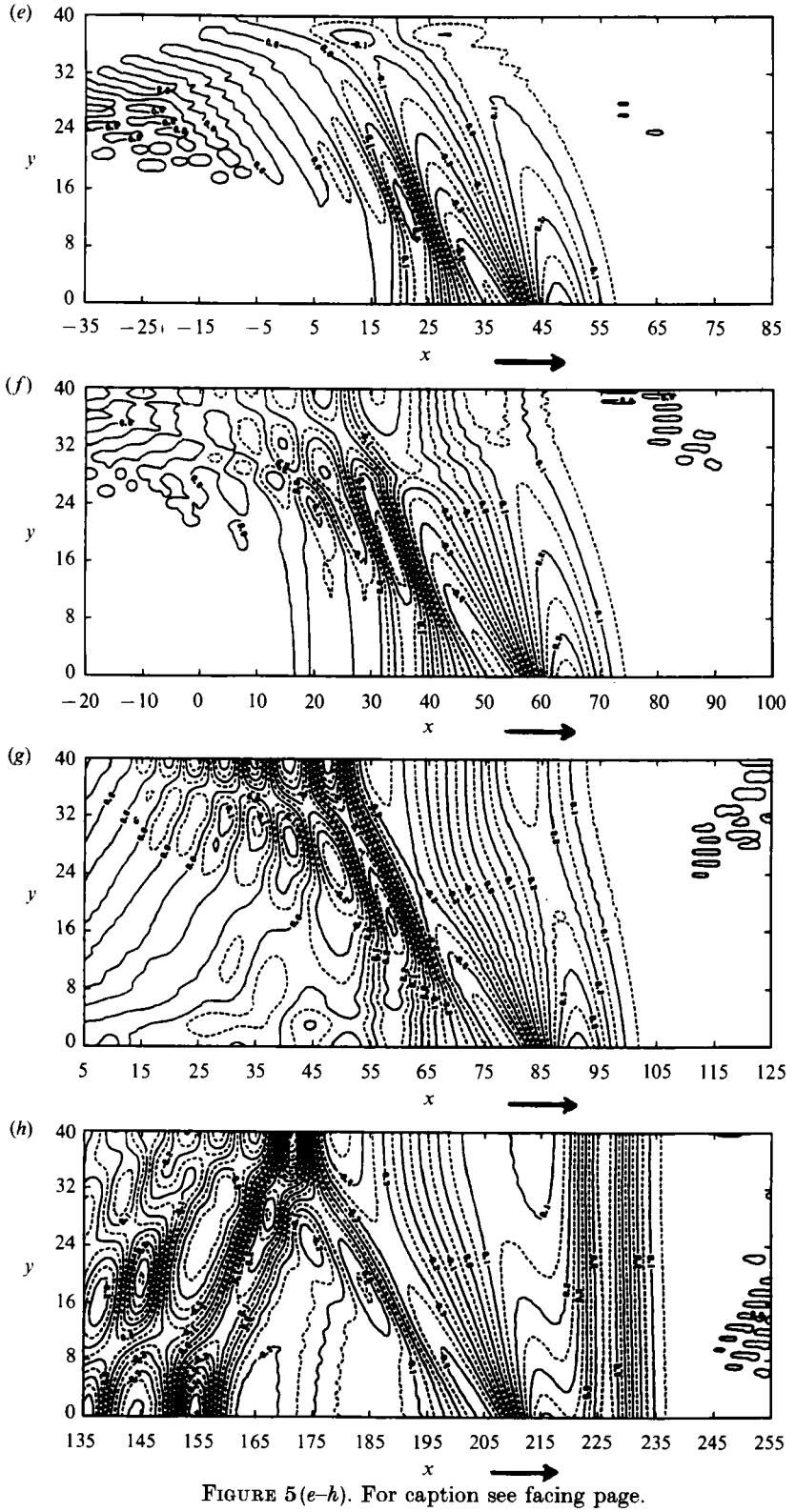

FIGURE 5(e–h). For caption see facing page.

	Subcritical		Transcritical	
Time	Linear θ	Nonlinear θ	Linear θ	Nonlinear θ
40	20°	20°	32°	34°
55	12°	12°	24°	29°
80	8°	8°	23°	22°
200	0°	0°	20°	0°

TABLE 1. The angle the leading crest makes at the centre of the channel with a line normal to the sidewalls for both the linear and nonlinear solutions for the subcritical ($F = 0.6$, $S = 0.044$, $W = 40$) and the transcritical case ($F = 1.05$, $S = 0.044$, $W = 40$).

parametric regimes (Grimshaw & Smyth 1986). The three types of upstream influence that are observed are shown in figure 6. Figure 7 summarizes the regions in the F–S (Froude number–Blockage coefficient) plane in which each type of solution is seen. Here results are given for three channel widths, $W = 20$, 30 and 40. Above a certain Froude number, called the limiting Froude number, no upstream influence is seen. Below $F = 1$, the upstream influence is an undular bore. In between the two, a train of equal amplitude solitary waves corresponding to the exact analytical solutions of the KdV equation given by (2.9), is generated and propagates upstream of the forcing. Both upstream advancing disturbances are essentially uniform and straight crested across the channel and correspond to solutions of the two-dimensional problem, i.e. the inhomogeneous KdV equation.

In figure 7 we have also plotted the corresponding regions for the two-dimensional problem. These agree quite well with the regions of the three-dimensional problem, with some modifications in accordance with the discussion in §4. In particular, the limiting Froude number is higher for the three-dimensional problem than the corresponding two-dimensional problem. To understand this difference, we look at the governing equation for the lowest transverse mode and write

$$\eta(x, y, t) = \bar{\eta}(x, t) + \tilde{\eta}(x, y, t), \tag{5.1}$$

where

$$\bar{\eta}(x, t) = \frac{1}{W}\int_0^W \eta(x, y, t)\,\mathrm{d}y \tag{5.2}$$

is the average of η across the channel (i.e. the lowest transverse mode), and $\tilde{\eta}$ consists of higher transverse modes. Substituting this into (3.2a) and integrating across the channel, using the boundary conditions (3.2c), gives

$$\bar{\eta}_t + \bar{\eta}_x + \bar{\eta}\bar{\eta}_x - \bar{\eta}_{xxt} = -\tfrac{3}{4}F\frac{B}{W}d_{-2}\,Y_\xi - \frac{\partial}{\partial x}\left[\frac{1}{2W}\int_0^W \tilde{\eta}^2\,\mathrm{d}y\right]. \tag{5.3}$$

We note that this is the governing equation for the corresponding two-dimensional case (see Appendix B, note the different scaling), modified by the additional forcing term on the right-hand side. Thus, the only influence of the higher transverse modes

FIGURE 5. Contour plots of the linear and quadratic nonlinear solution for η for the transcritical case ($F = 1.05$, $S = 0.044$, $W = 40$). (*a*) Linear at $t = 40$; (*b*) linear at $t = 55$; (*c*) linear at $t = 80$; (*d*) linear at $t = 200$; (*e*) nonlinear at $t = 40$; (*f*) nonlinear at $t = 55$; (*g*) nonlinear at $t = 80$; (*h*) nonlinear at $t = 200$. The arrows indicate the location, size and direction of propagation of the sidewall constriction.

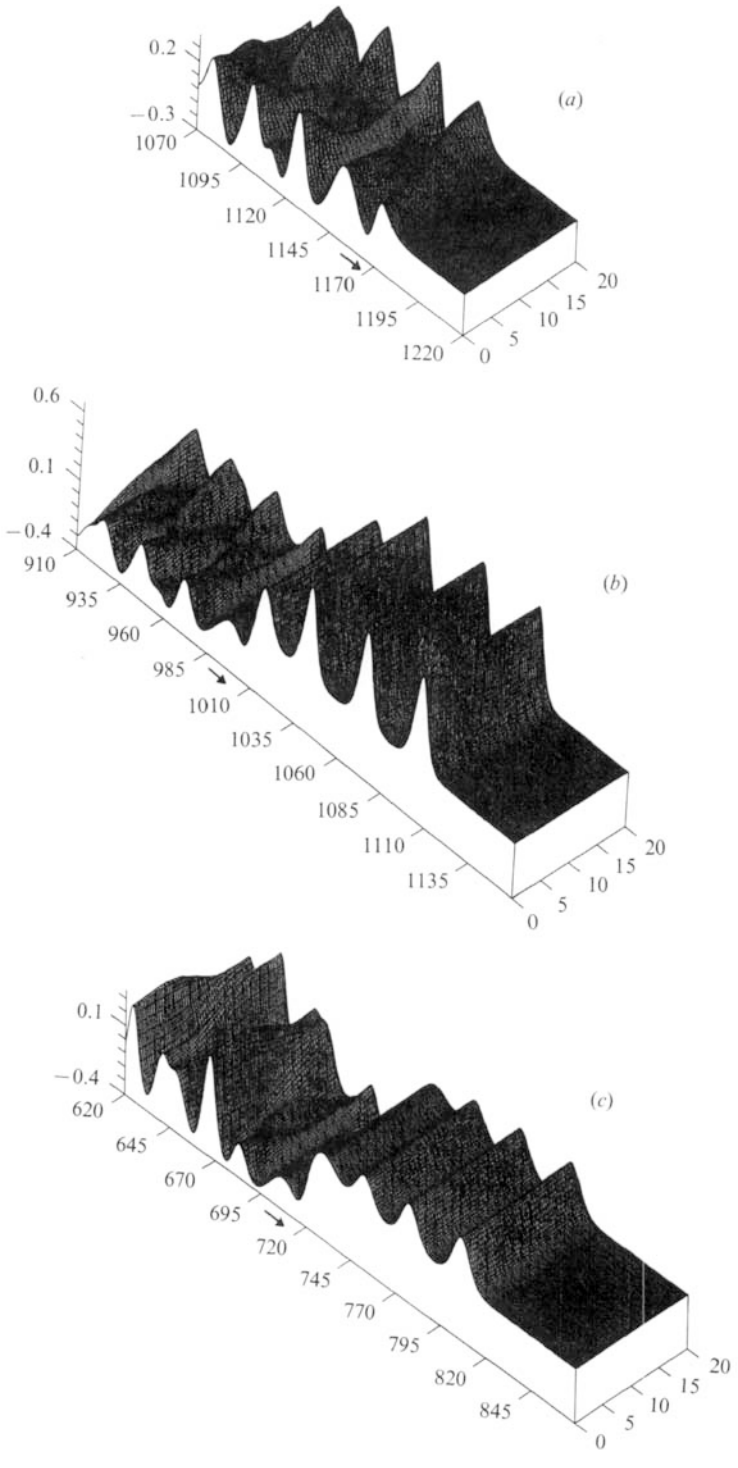

FIGURE 6. The three types of upstream influence observed in the quadratic nonlinear problem. (*a*) No upstream influence. (*b*) Upstream solitary waves. (*c*) Upstream undular bore. The arrows indicate the location, size and direction of propagation of the sidewall constriction.

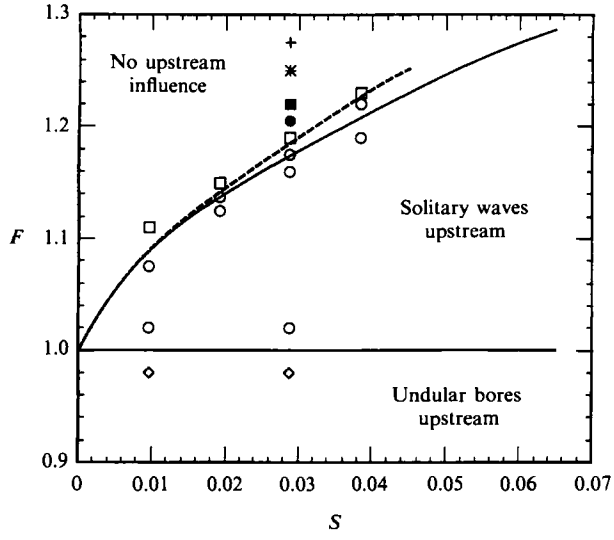

FIGURE 7. Regions in the F–S plane occupied by the different upstream solution types in the quadratic nonlinear problem. ——, Two-dimensional boundaries; – – –, three-dimensional boundaries for $W = 20$; □, no upstream influence for $W = 20$; ○, solitary waves upstream for $W = 20$; ◇, undular bore upstream for $W = 20$; ■, no upstream influence for $W = 30$; ●, solitary waves upstream for $W = 30$; +, no upstream influence for $W = 40$; *, solitary waves upstream for $W = 40$.

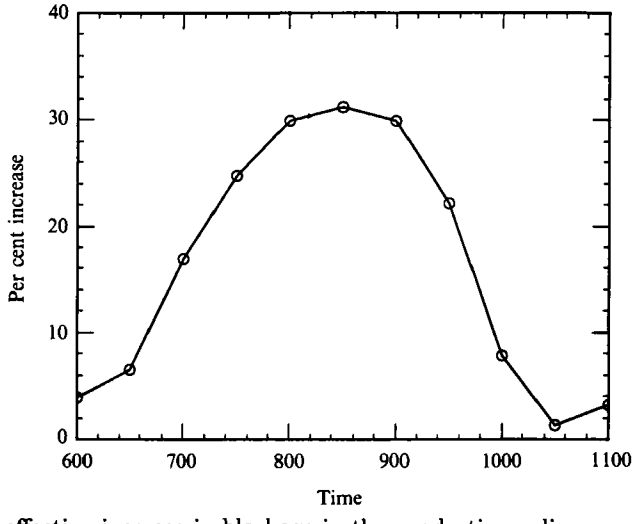

FIGURE 8. The effective increase in blockage in the quadratic nonlinear case over one cycle of soliton generation. Here $W = 30$, $F = 1.175$ and $S = 0.0288$.

on the evolution of the lowest mode is to provide an additional forcing term, which can be interpreted as an equivalent additional constriction equal to

$$(BY)_{\mathrm{eq}} = \frac{2}{3}\frac{1}{Fd_{-2}}\int_0^W \tilde{\eta}^2(x, y, t)\,\mathrm{d}y, \tag{5.4}$$

thus changing the effective blockage coefficient for $\bar{\eta}(x, t)$ from that for the two-dimensional case.

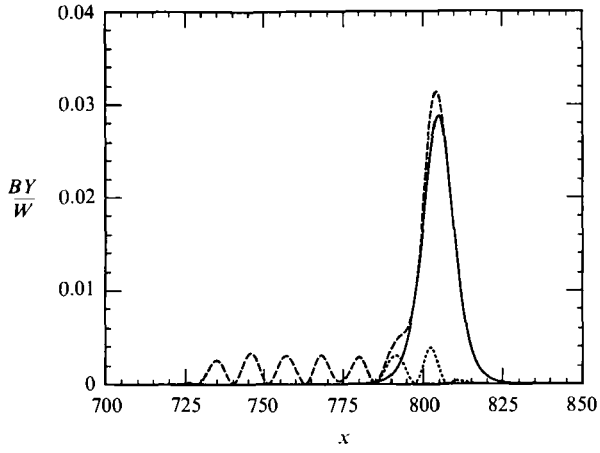

FIGURE 9. An example of the increased blockage in the quadratic nonlinear case. Here $W = 20$, $F = 1.175$ and $S = 0.0288$. ——, Physical constriction; ..., additional equivalent constriction; – – –, total effective constriction.

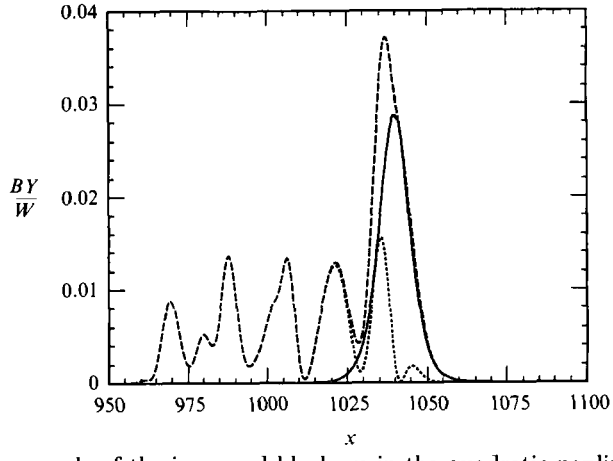

FIGURE 10. An example of the increased blockage in the quadratic nonlinear case. Here $W = 30$, $F = 1.175$ and $S = 0.0288$. ——, Physical constriction; ..., additional equivalent constriction; – – –, total effective constriction.

The equivalent additional constriction was found to be unsteady, resulting in fluctuations in the size of the total constriction with time. Figure 8 shows how the effective increase in the blockage changes through one cycle of soliton generation for $W = 30$, $F = 1.175$ and $S = 0.0288$. In figure 9 we give an example of the increased effective blockage for $W = 20$, $F = 1.175$ and $S = 0.0288$, showing about a 10% increase in blockage, which is close to the maximum increase observed for these conditions. This increase was found to depend on the width of the channel, becoming larger as the width of the channel increased, while keeping the physical blockage coefficient constant. In figure 10 we give an example of the increased effective blockage for $W = 30$, again for $F = 1.175$ and $S = 0.0288$, showing about a 30% increase in blockage, which again is close to the maximum increase seen for these conditions (see figure 8). This is consistent with Pedersen's (1988) findings of the limiting Froude number increasing with increased amplitude of the constriction, again with the physical blockage coefficient kept constant.

The observed increase in the limiting Froude number for $S = 0.0288$ from $F = 1.175$ to $F = 1.185$ for $W = 20$ and $F = 1.21$ for $W = 30$ (see figure 7) is consistent with approximately 10% and 30% increase in blockage for the two-dimensional case, respectively (see figure 7), agreeing well with the increase seen in effective blockage in the three-dimensional case. However, it should be kept in mind that the two-dimensional results apply to a steady, constant shape constriction, whereas the effective three-dimensional constriction fluctuates in size and shape. Thus any comparison between the two has to be more qualitative than quantitative.

6. Results for cubic nonlinearity

If the two layer depths are comparable, cubic terms become comparable to quadratic terms and thus cannot be neglected. Formally this corresponds to $d_+ - d_- = O(\alpha)$. In figure 11 we have plotted the ratio of the quadratic to cubic nonlinear terms in (2.1a) for different strengths of the nonlinearity. We see that even for moderate nonlinearities, cubic nonlinearity is important for a range of depths around $d_+ = d_-$, and as the nonlinearity strengthens this range becomes larger.

For small times the nonlinear solutions for the transcritical case with cubic nonlinearity shown in figure 12 agree well with the linear ones and the quadratic nonlinear ones given in figure 5, again confirming the dominance of linear dynamics over nonlinear ones at these small times (here we have taken $d_-^*/(d_-^* + d_+^*) = 0.35$, giving $\gamma = 4.70$ in (3.2a)). As time increases, nonlinear effects become important and as before, in certain parametric regimes, we see two-dimensional, straight-crested nonlinear waves propagating upstream of the forcing, again in accordance with the arguments given in §4 on the importance of the lowest transverse mode.

However, the types of upstream influence observed are now different from those seen in §5. These are shown in figure 13 and the corresponding regions in the F–S plane in which each solution type is seen are plotted in figure 14. Here, results are given for $W = 20$ only ($W = 30$ and $W = 40$ gave the same results up to the accuracy that our discrete set of runs provides). These regions correspond exactly to those seen in the two-dimensional solutions, i.e. from solving the inhomogeneous EKdV equation (Melville & Helfrich 1987). Above a certain Froude number there is no upstream influence. Below a certain Froude number the upstream advancing disturbance is an undular bore, very much like the quadratic nonlinear case. However, in the region between those two, rather than seeing a train of solitary waves, we observe an upstream advancing monotonic bore. This front-like solution corresponds locally to the exact solution of the EKdV equation, given by (2.10).

Unlike the quadratic nonlinear case, the boundaries in the F–S plane were found to be the same for the three-dimensional case as those for the two-dimensional case and consequently independent of the width of the channel. This holds at least to the accuracy that we were able to determine these boundaries from our discrete set of runs, as indicated by the symbols in figure 14. Trying to determine the boundaries more accurately proved to be too expensive computationally owing to the large times needed as we approach the boundaries. This good agreement is easily understandable for the limiting Froude number, since it is directly determined by the speed of the monotonic front solution, which in turn is dictated by the stratification parameters of the problem, as discussed in §2. To understand the agreement for the boundary between monotonic and undular bores upstream, we can look at the evolution equation for the lowest mode, as we did in §5 for the quadratic case. Following that analysis, using (5.1) and (5.2), substituting into (3.2a), integrating across the channel

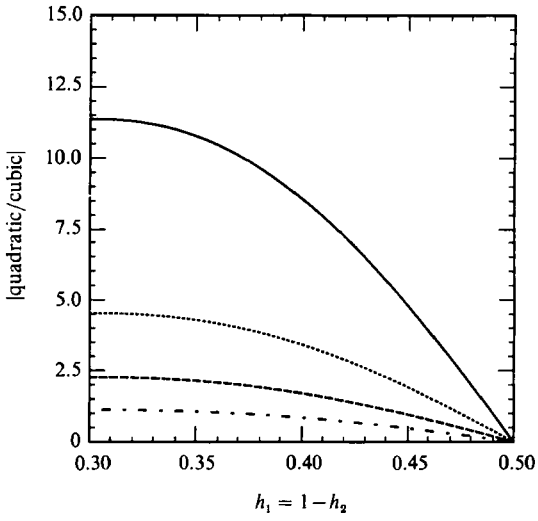

FIGURE 11. The ratio of the quadratic and cubic nonlinear terms in the coupled evolution equation as a function of the normalized upper-layer depth for different strengths of the nonlinearity. ——, $\alpha = 0.01$; ..., $\alpha = 0.025$; – – –, $\alpha = 0.05$; –·–, $\alpha = 0.1$. Note that here $h_{1,2} = d^*_{+,-}/h$ and $\alpha = a/h$, where $h = d^*_+ + d^*_-$ is the total depth.

and isolating the corresponding two-dimensional operator on the left-hand side, we obtain, corresponding to (5.4), the following equivalent additional constriction

$$(BY)_{\text{eq}} = \frac{2}{3}\frac{1}{Fd_{-2}}\left\{\int_0^W \tilde{\eta}^2\,\mathrm{d}y - 2\gamma\bar{\eta}\int_0^W \tilde{\eta}^2\,\mathrm{d}y - \tfrac{2}{3}\gamma\int_0^W \tilde{\eta}^3\,\mathrm{d}y\right\}, \tag{6.1}$$

where the two additional terms are due to cubic nonlinear effects. From the dominance of the first transverse mode ($n = 1$) in the solution for $\tilde{\eta}$ (see figure 4), we immediately see that the last term will in general be much smaller than the other two in the region of the physical constriction, and can thus be neglected. Recalling our scaling, the first two terms will be of the same order of magnitude, however, they are of opposite sign in the region of interest, since there $\bar{\eta} > 0$. Thus the two terms will tend to balance each other, reducing the effect of the additional constriction from that in the quadratic nonlinear case. This was tested for several conditions, all of which showed very little or no increase in the effective blockage from the two-dimensional case.

7. Discussion

In this paper we have attributed the two-dimensionality of the upstream waves generated by a transcritical flow past a constriction in a channel to properties of the linear modes, as well as nonlinear effects. Decomposing the problem using the linear transverse modes, which form a complete and orthogonal set, has proved helpful in understanding the underlying dynamics, exposing the different evolution processes of the lowest transverse mode on one hand and the higher transverse modes on the other. In the transcritical range of Froude numbers, the lowest mode evolves in much the same way as the two-dimensional problem, generating nonlinear waves upstream through resonant effects, whereas the dispersive properties prevent the higher modes from producing waves upstream.

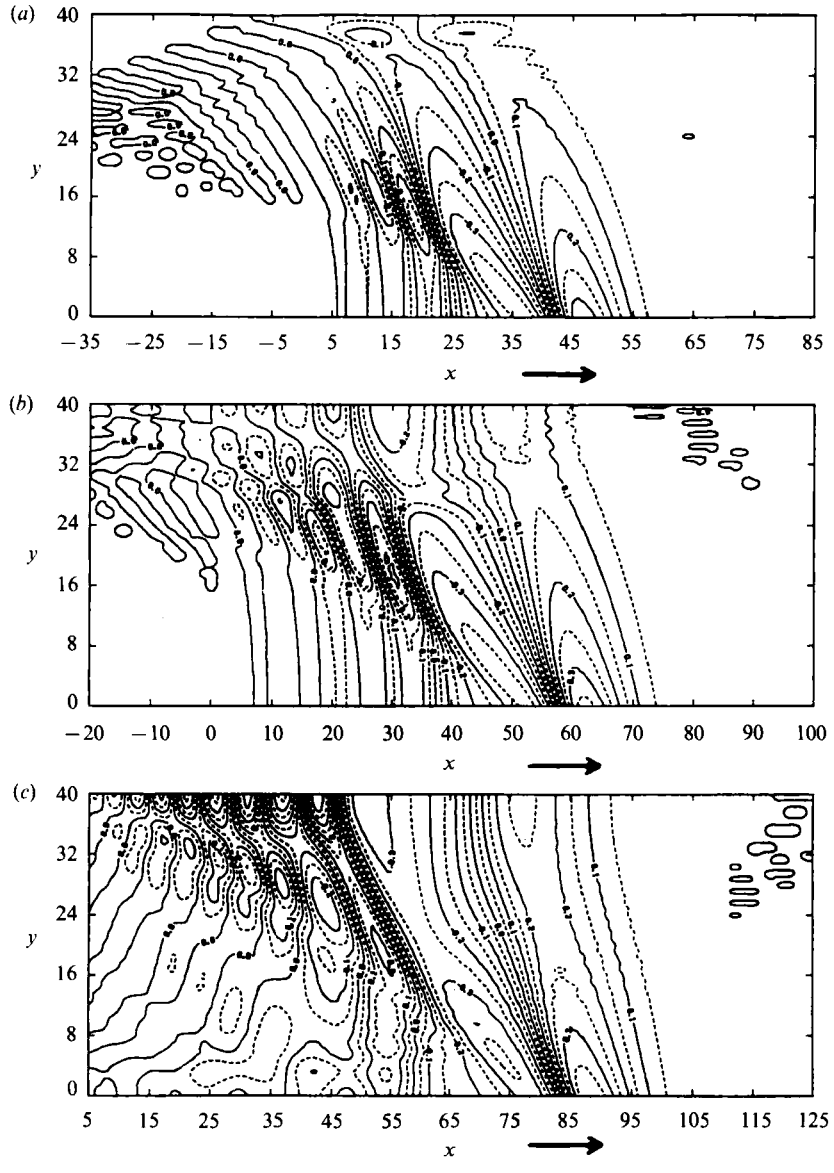

FIGURE 12. Contour plots of the cubic nonlinear solution for η. (*a*) $t = 40$; (*b*) $t = 55$; (*c*) $t = 80$. The arrows indicate the location, size and direction of propagation of the sidewall constriction. Here $d_-^*/(d_-^* + d_+^*) = 0.35$ giving $\gamma = 4.70$.

These ideas carry over to the problem of upstream influence in a rotating channel, where the Kelvin mode may evolve nonlinearly upstream, whereas the Poincaré modes may not produce any upstream influence. However, this situation is complicated by the fact that the upstream advancing Kelvin wave may act as a transcritical forcing for the linear Poincaré modes, as shown by Melville, Tomasson & Renouard (1989). This results in the nonlinear Kelvin wave becoming unstable owing to resonant forcing of the Poincaré waves, with the crest curving backwards and the amplitude decreasing as it propagates along the channel, as was observed in experiments by Melville, Renouard & Zhang (1990), who towed a body at transcritical speeds through a rotating two-layer fluid.

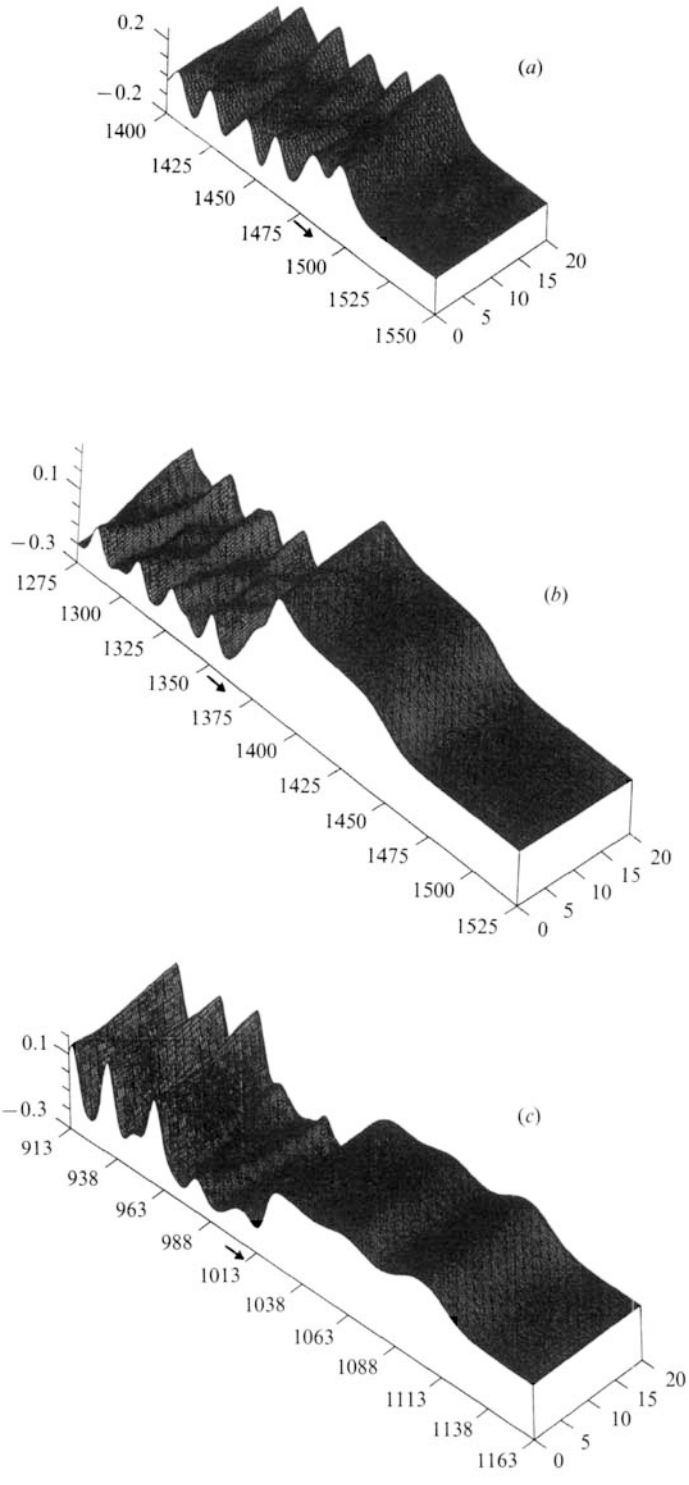

FIGURE 13. The three types of upstream influence observed in the cubic nonlinear problem. (*a*) No upstream influence. (*b*) Upstream monotonic bore. (*c*) Upstream undular bore. The arrows indicate the location, size and direction of propagation of the sidewall constriction.

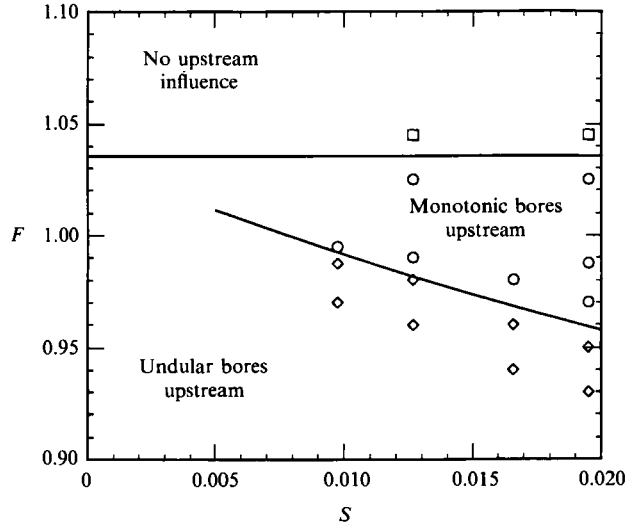

FIGURE 14. Regions in the F–S plane occupied by the different upstream solution types in the cubic nonlinear problem. ——, Two-dimensional boundaries; □, no upstream influence for $W = 20$; ○, monotonic bore upstream for $W = 20$; ◇, undular bore upstream for $W = 20$. Here $d_-^*/(d_-^* + d_+^*) = 0.35$ giving $\gamma = 4.70$.

Finally, it should be emphasized that these results apply only to channels of intermediate width, or more precisely with $kW = O(\beta^{-\frac{1}{2}})$. As W increases, the separation between the dispersion curves of the transverse modes decreases (see figure 1), resulting in the curves moving closer to the forcing curve. Thus a clear separation of a nonlinearly evolving lowest mode from linearly evolving higher modes is not possible.

This work was supported by the Office of Naval Research (Coastal Sciences).

Appendix A. Evolution equations for a single-layer fluid

To derive coupled evolution equations for a homogeneous fluid with a free surface, we take the scaling to be

$$\left.\begin{aligned} x^* = k^{-1}x, \quad y^* = l^{-1}y, \quad t^* = (kc_0)^{-1}t, \\ \eta^* = a\eta, \quad c_0^2 = gh, \end{aligned}\right\} \tag{A 1}$$

instead of that given by (2.3). Following a derivation similar to that outlined in §2, we obtain the coupled evolution equations

$$\eta_t + \eta_x + \tfrac{3}{2}\alpha\eta\eta_x - \tfrac{1}{6}\beta\eta_{xxt} + \tfrac{1}{2}\Gamma V_y = 0, \tag{A 2a}$$

$$V_t + \eta_y = 0, \tag{A 2b}$$

where $\alpha = a/h$, $\beta = (kh)^2$ and $\Gamma = (l/k)^2$ are the small parameters, h is the equilibrium depth of the fluid, η is the surface displacement and V is the depth averaged transverse velocity. The boundary conditions are

$$V = -\frac{FB}{\alpha\Gamma}\frac{\mathrm{d}Y}{\mathrm{d}\xi} \quad \text{at} \quad y = 0, \tag{A 3a}$$

$$V = 0 \quad \text{at} \quad y = W, \tag{A 3b}$$

where $y = BY(\xi)$ defines the right-hand wall, B is the maximum amplitude of the constriction and $\xi = x - Ft$. The blockage coefficient for this single-layer case is

$$S = \frac{B}{W}. \tag{A 4}$$

Renormalizing the two-layer evolution equations (2.1*a b*) (without the cubic nonlinear term), together with the boundary conditions (2.4*a*, *b*), using

$$\left.\begin{aligned} \eta = d_{-2}\eta', \quad V = d_{-2}V', \\ t = \frac{t'}{(d_1)^{\frac{1}{2}}}, \quad x = \frac{x'}{(d_1)^{\frac{1}{2}}}, \quad y = \frac{y'}{(d_1)^{\frac{1}{2}}}, \end{aligned}\right\} \tag{A 5}$$

where the primed variables correspond to those used in §2, results in

$$\eta_t + \eta_x + \tfrac{3}{2}\alpha\eta\eta_x - \tfrac{1}{6}\beta\eta_{xxt} + \tfrac{1}{2}\Gamma V_y = 0, \tag{A 6a}$$

$$V_t + \eta_y = 0, \tag{A 6b}$$

with the boundary conditions

$$V = -\frac{FB}{\alpha\Gamma} d_{-2} \frac{\mathrm{d}Y}{\mathrm{d}\xi} \quad \text{at} \quad y = 0, \tag{A 7a}$$

$$V = 0 \quad \text{at} \quad y = W. \tag{A 7b}$$

Here B is the maximum amplitude of Y, $BY = (Y_- - Y_+)$. Comparing the two systems of equations, we see that they are formally equivalent, given that we take the blockage coefficient for the two-layer case to be

$$S = \frac{B}{W} d_{-2}. \tag{A 8}$$

Appendix B. The corresponding two-dimensional problem

By assuming the solution for η to be two-dimensional, i.e.

$$\eta(x, y, t) = \bar{\eta}(x, t), \tag{B 1}$$

we get, after substituting into (2.1*a*) and integrating across the channel, using the boundary conditions (2.4)

$$\bar{\eta}_t + \bar{\eta}_x + \tfrac{3}{2}\alpha[d_{-2}\bar{\eta} - 2\alpha d_{-3}\bar{\eta}^2]\bar{\eta}_x - \tfrac{1}{6}\beta d_1 \bar{\eta}_{xxt} = -\frac{F}{2\alpha} B \frac{\mathrm{d}Y}{\mathrm{d}\xi}, \tag{B 2}$$

which is the equation solved by Melville & Helfrich (1987) and we refer to as the corresponding two-dimensional problem.

REFERENCES

Akylas, T. R. 1984 On the excitation of long nonlinear water waves by a moving pressure distribution. *J. Fluid Mech.* **141**, 455–466.

Baines, P. G. 1984 A unified description of two-layer flow over topography. *J. Fluid Mech.* **140**, 127–167.

Ertekin, R. C. 1984 Soliton generation by moving disturbances in shallow water: Theory, computation and experiment. PhD thesis, University of California, Berkeley.

ERTEKIN, R. C., WEBSTER, W. C. & WEHAUSEN, J. V. 1984 Ship generated solitons. *Proc. 15th Symp. Naval Hydrodynamics*, pp. 1–15. National Academy of Sciences, Washington, D.C.

ERTEKIN, R. C., WEBSTER, W. C. & WEHAUSEN, J. V. 1986 Waves caused by a moving disturbance in a shallow channel of finite width. *J. Fluid Mech.* **169**, 275–292.

GRIMSHAW, R. & MELVILLE, W. K. 1989 On the derivation of the modified Kadomtsev–Petviashvili equation. *Stud. Appl. Maths* **80**, 183–202.

GRIMSHAW, R. H. J. & SMYTH, N. F. 1986 Resonant flow of a stratified fluid over topography. *J. Fluid Mech.* **169**, 429–464.

HELFRICH, K. R. & MELVILLE, W. K. 1990 Review of dispersive and resonant effects in internal wave propagation. In *The Physical Oceanography of Sea Straits* (ed. L. J. Pratt), pp. 391–420. Kluwer.

HUANG, D.-B., SIBUL, O. J., WEBSTER, W. C., WEHAUSEN, J. V., WU, D.-M. & WU, T. Y. 1982 Ships moving in a transcritical range. *Proc. Conf. on Behaviour of Ships in Restricted Waters (Varna, Bulgaria)*, vol. 2, pp. 26-1–26-10.

KAKUTANI, T. & YAMASAKI, N. 1978 Solitary waves on a two-layer fluid. *J. Phys. Soc. Japan* **45**, 674–679.

KATSIS, C. & AKYLAS, T. R. 1987 On the excitation of long nonlinear water waves in a moving pressure distribution. Part 2. Three-dimensional effects. *J. Fluid Mech.* **177**, 49–65.

MACOMB, E. S. 1986 The interaction of nonlinear waves and currents with coastal topography. SM thesis, Department of Civil Engineering, MIT.

MEI, C. C. 1986 Radiation of solitons by slender bodies advancing in a shallow channel. *J. Fluid Mech.* **162**, 53–67.

MELVILLE, W. K. & HELFRICH, K. R. 1987 Transcritical two-layer flow over topography. *J. Fluid Mech.* **178**, 31–52.

MELVILLE, W. K. & MACOMB, E. 1987 Transcritical stratified flow in straits. *Preprints of the Third International Symposium on Stratified Flows* (ed. J. List). California Institute of Technology.

MELVILLE, W. K., RENOUARD, D. P. & ZHANG, X. 1990 On the generation of nonlinear Kelvin waves in a rotating channel. *J. Geophys. Res.* **95** (C10), 18247–18254.

MELVILLE, W. K., TOMASSON, G. G. & RENOUARD, D. P. 1989 On the stability of Kelvin waves. *J. Fluid Mech.* **206**, 1–23.

MILES, J. W. 1977 Resonantly interacting solitary waves. *J. Fluid Mech.* **79**, 171–179.

MILES, J. M. 1979 On internal solitary waves. *Tellus* **31**, 456–462.

MILES, J. W. 1980 Solitary waves. *Ann. Rev. Fluid Mech.* **12**, 11–43.

PEDERSEN, G. 1988 Three-dimensional wave patterns generated by moving disturbances at transcritical speeds. *J. Fluid Mech.* **196**, 39–63.

SMYTH, N. F. 1987 Modulation theory solution for resonant flow over topography. *Proc. R. Soc. Lond.* A **409**, 79–97.

TOMASSON, G. G. 1988 On the stability of long nonlinear Kelvin waves. SM thesis, Department of Civil Engineering, MIT.

WHITHAM, G. B. 1974 *Linear and nonlinear waves*. Wiley.

WINTHER, R. 1983 Model equations for long, almost plane waves in nonlinear dispersive systems. Unpublished manuscript, University of Oslo.

WU, D.-M. & WU, T. Y 1982 Three-dimensional nonlinear long waves due to moving surface pressure. In *Proc. 14th Symp. Naval Hydrodynamics*, pp. 103–129. National Academy of Sciences, Washington, D.C.

WU, T. Y. 1987 Generation of upstream advancing solitons by moving disturbances. *J. Fluid Mech.* **184**, 75–99.